

X-RAY AND GAMMA-RAY EMISSION FROM PULSAR MAGNETOSPHERES

J. Dyks, B. Rudak

Nicolaus Copernicus Astronomical Center, Rabiańska 8, 87-100 Toruń, Poland

ABSTRACT For polar-cap models based on electromagnetic cascades induced by curvature radiation of beam particles we calculate broad-band high-energy spectra of pulsed emission expected for classical ($\sim 10^{12}$ G) and millisecond pulsars ($\sim 10^9$ G). The spectra are a superposition of curvature and synchrotron radiation components and most of their detailed features depend significantly on the magnetic field strength. The relations of expected pulsed luminosity L_X (between 0.1 keV and 10 keV) as well as L_γ (above 100 keV) to the spin-down luminosity L_{sd} are presented. We conclude that spectral properties and fluxes of pulsed non-thermal X-ray emission of some objects, like the Crab or the millisecond pulsar B1821–24, pose a challenge to the polar-cap models based on curvature and synchrotron radiation alone. On the other hand, such models may offer an explanation for the case of B1706–44.

KEYWORDS: pulsars; X-rays; gamma-rays.

1. INTRODUCTION

The aim of this paper is to present general features of broad-band $X\gamma$ spectra expected for polar cap models with $X\gamma$ emission due to curvature (CR) and synchrotron (SR) processes (e.g. Daugherty & Harding 1982, Daugherty & Harding 1996) and to show that the luminosity of pulsed X-rays L_X inferred for some pulsars is too high when compared to their gamma-ray luminosity L_γ (or to their spin-down luminosity L_{sd} when there is no information about gamma-rays) to be understood within polar-cap models unless some unorthodox assumptions are accepted. Some of these features are only weakly model-dependent and may, therefore, play a decisive role in assessing validity of polar-cap models. Details of the results presented below are given by Rudak & Dyks (1998b).

2. SPECTRAL PROPERTIES OF CURVATURE RADIATION

For a monoenergetic injection rate function Q_e of beam particles cooled via CR, their steady-state energy distribution (of a form $N_e \propto \gamma^{-4}$) ranges from an injection energy γ_0 down to some lower limit γ_{break} , determined by the condition, that a cooling time-scale due to CR, t_{cr} , is shorter than a time-scale for the particle to reside in the region of efficient CR cooling, t_{esc} . The corresponding photon spectrum of CR has a form: $N_{cr}(\epsilon) \propto \epsilon^{-\frac{5}{3}}$ and extends from $\epsilon_{cr}(\gamma_0)$ down to $\epsilon_{break} \equiv \epsilon_{cr}(\gamma_{break})$ where $\epsilon_{cr}(\gamma) = 1.5 c \hbar \gamma^3 \rho_{cr}^{-2}$ (ρ_{cr} is a radius of local curvature). Below ϵ_{break} the photon spectrum follows the low energy tail of CR: $N_{cr}(\epsilon) \propto \epsilon^{-\frac{2}{3}}$.

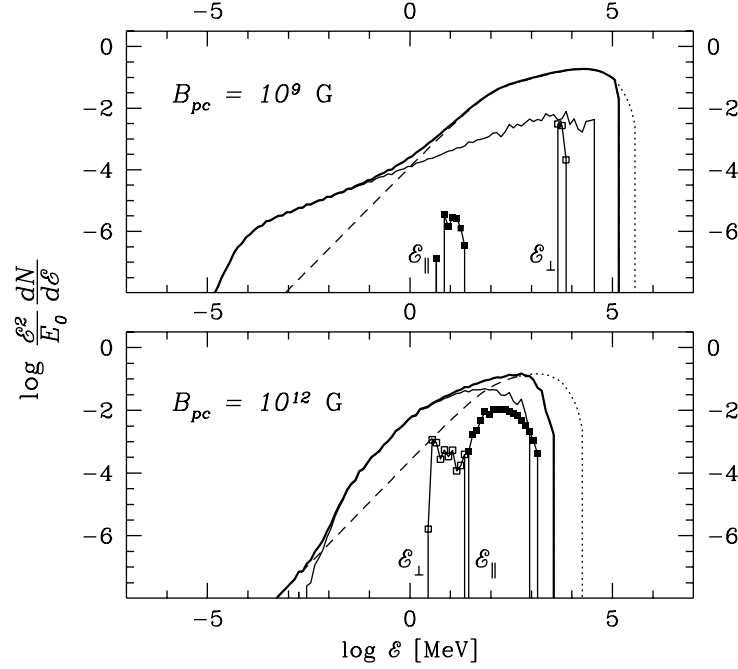


FIGURE 1. The radiation energy spectrum per logarithmic bandwidth (thick solid line). The spectrum is normalized to the energy of the parent particle, E_0 . Dashed line represents its CR component, part of which (dotted line) has been reprocessed by magnetic absorption into e^\pm -pairs. Thin solid line is the SR component. In addition to the electromagnetic spectra, we show the spectra of e^\pm -pairs: the line connecting filled squares is for the energy parallel to local magnetic field lines ($\mathcal{E}_\parallel = \gamma_\parallel m_e c^2$); the line connecting open squares is the initial distribution of energy perpendicular to local magnetic lines ($\mathcal{E}_\perp = \gamma_\perp m_e c^2$). The upper panel is for $B_{pc} = 10^9$ G, $P = 3.1 \times 10^{-3}$ s (i.e. $L_{sd} = 10^{35}$ erg s $^{-1}$) and $E_0 = 1.08 \times 10^7$ MeV. The lower panel is for $B_{pc} = 10^{12}$ G, $P = 5.6 \times 10^{-2}$ s (i.e. $L_{sd} = 10^{36}$ erg s $^{-1}$) and $E_0 = 6.68 \times 10^6$ MeV.

To find γ_{break} analytically, we can approximate t_{esc} with ρ_{cr}/c and from the condition $t_{\text{cr}} = t_{\text{esc}}$ we obtain the photon energy at which the spectral break should occur: $\epsilon_{\text{break}} = \frac{9}{4} \hbar e^{-2} m_e c^3 \approx 150$ MeV. It does not depend on any pulsar parameters (in particular, on magnetic field structure) as long as our estimate of t_{esc} is accurate.

The CR component, dominating the gamma-ray domain, is visible in both panels of Fig.1 which show numerically calculated spectra of both CR and SR (and with transfer effects due to magnetic absorption included) per beam particle of initial energy E_0 (Rudak & Dyks 1998a), injected at the polar cap's rim of a pulsar with a dipolar magnetic field of $B_{pc} = 10^9$ G (upper panel), and $B_{pc} = 10^{12}$ G (lower panel). The spectral break at around 100 MeV is particularly pronounced in the former case.

3. SPECTRAL PROPERTIES OF SYNCHROTRON RADIATION

The synchrotron radiation is emitted by e^\pm -pairs created in the process of magnetic absorption of high-energy photons. The character of the source function Q_\pm of e^\pm -pairs depends primarily on the distribution of their pitch angles ψ and on the richness of the cascades. In contrast to outer-gap models, small opening angles of magnetic field lines above the polar cap result in confinement of pitch angles to a narrow range of low values.

In the case of $B_{\text{pc}} = 10^9$ G (Fig.1, upper panel) only one generation of e^\pm -pairs is produced. Their source function Q_\pm is almost monoenergetic and the steady-state energy distribution of SR-cooled pairs ($N_\pm \propto \gamma_\perp^{-2}$) results in photon spectrum of SR with a well known power-law shape $N_{\text{sr}}(\epsilon) \propto \epsilon^{-\frac{3}{2}}$. This spectrum extends down to a low-energy turnover ϵ_{ct} determined by the condition $\gamma_\perp \approx 1$ (O'Dell & Sartori 1970). Below the turnover energy ϵ_{ct} , located around 0.1 keV, the spectrum flattens, and may be described asymptotically as $N_{\text{sr}}(\epsilon) \propto \epsilon^{+1}$. The SR component dominates over the CR component below ~ 1 MeV, i.e. over the entire X-ray energy band.

In the case of $B_{\text{pc}} = 10^{12}$ G (Fig.1, lower panel) the SR component dominates over the CR in the energy range of soft gamma-rays and hard X-rays. The spectrum of the source function Q_\pm of secondary pairs is spread over two decades in energy. Therefore, instead of a single, well defined turnover energy, the SR spectrum reveals a gradual turnover which starts at ~ 1 MeV (due to high values of γ_\parallel as well as strong local B). At about 10 keV the SR component falls below the level of the CR component.

Although for 10^9 G the spectrum of SR extends well into the soft X-ray band and dominates there, its fractional contribution to the total radiation energy output is low. It varies between 0.003 (for $L_{\text{sd}} = 10^{34}$ erg s $^{-1}$) and 0.22 (for 10^{37} erg s $^{-1}$). For the case of 10^{12} G, the energy content of SR becomes significant for $L_{\text{sd}} > 10^{33}$ erg s $^{-1}$, but the spectrum of SR is now confined to gamma-rays, and it turns over at $\lesssim 1$ MeV. In either case, the bulk of particle energy is converted into radiation concentrated within the gamma-ray energy band.

4. RELATIONS BETWEEN X-RAY AND γ -RAY LUMINOSITIES

The spectra calculated for a wide range of periods and magnetic fields show that the energy band of X-rays is never energetically important. Fig.2 presents X-ray and gamma-ray luminosities (L_γ and L_x) as a function of L_{sd} , calculated by integrating the numerical spectra. Predicted values of L_x do not follow the empirical relation $L_x(L_{\text{sd}})$ found by Saito et al.(1988) for pulsed components of X-ray emission. The calculated ratio L_x/L_γ remains at the level between 10^{-6} and 10^{-4} , in disagreement with observations. For the Crab, the observed ratio of L_x/L_γ is about 0.47 (with L_x and L_γ inferred for $\Omega_x = \Omega_\gamma = 1$ sr). B1821–24, a ‘Crab-like’ millisecond object, also poses a challenge to the polar-cap models. Apart from the disagreement between the observed and predicted spectral slopes

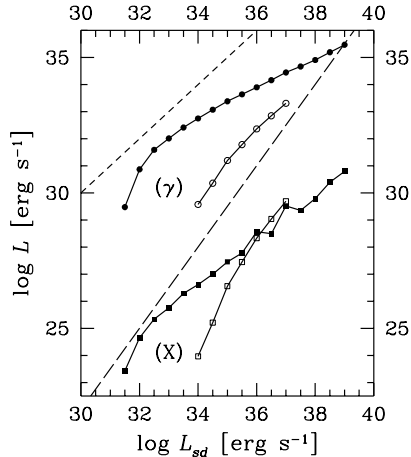


FIGURE 2. Evolution of high-energy, non-thermal luminosity across the spin-down luminosity space. The long upper curve connecting filled dots is the track of gamma-ray luminosity $L_\gamma (> 100 \text{ keV})$, and the long lower curve connecting filled squares is the track of X-ray luminosity $L_X (0.1 - 10 \text{ keV})$, both calculated for a pulsar with $B_{\text{pc}} = 10^{12} \text{ G}$. The short upper curve with open circles is for L_γ , and the short lower curve with open squares is for L_X , calculated for $B_{\text{pc}} = 10^9 \text{ G}$. The short-dashed line marks $L = L_{\text{sd}}$. The long-dashed line, marking the empirical relation of Saito et al. (1998) has been added for reference.

(photon index $\simeq 1.9$ (Saito et al. 1997) and 1.2, respectively) the predicted ratio $L_X/L_\gamma \simeq 2 \times 10^{-4}$ would make L_γ larger than L_{sd} .

On the other hand, the extremely low predicted ratios of L_X/L_γ may offer an explanation for the case of B1706–44, a strong gamma-ray pulsar detected with *EGRET* ($L_\gamma = 2.5 \times 10^{34} \text{ erg s}^{-1}$, Thompson et al. 1996) which shows no pulsed X-ray emission. Its steady X-ray emission with $L_X = 1.3 \times 10^{33} \text{ erg s}^{-1}$ (Becker et al. 1995), probably of nebular origin, far exceeds the level of the predicted pulsed component: $L_X \approx 3 \times 10^{29} \text{ erg s}^{-1}$.

ACKNOWLEDGMENTS

This work has been financed by the KBN grant 2P03D-00911. BR acknowledges travel grants 2P03C00511p01 and 2P03C00511p04.

REFERENCES

- Becker W., Brazier K.T.S., Trümper J., 1995, A&A, 298, 528
- Becker W., Trümper J., 1997, A&A, 326, 682
- Daugherty J.K., Harding A.K., 1982, ApJ, 252, 337
- Daugherty J.K., Harding A.K., 1996, ApJ, 458, 278
- O’Dell S.L., Sartori L., 1970, ApJ, 161, L63
- Rudak B., Dyks J., 1998a, MNRAS, 295, 337
- Rudak B., Dyks J., 1998b, MNRAS, submitted
- Saito Y., Kawai N., Kamae T., Shibata S., 1998, in Proc. of the International Conference on Neutron Stars and Pulsars, eds. Shibasaki N., Kawai N. et al., Universal Academy Press, Tokyo, 295
- Saito Y. et al., 1997, ApJ, 477, L37
- Thompson D.J. et al., 1996, ApJ, 465, 385